Modeling in Organotin Chemistry Using NMR Restraints: A Case Study on the 9*R*,12*S*-$[tBu_2Sn]_2O$ Derivative of Erythromycin A

José C. Martins,*,† Rudolph Willem,†,‡ Frédéric A. G. Mercier,†,‡ Marcel Gielen,‡ and Monique Biesemans†,‡

Contribution from the High-Resolution NMR Center (HNMR) and General and Organic Chemistry Department (AOSC), Vrije Universiteit Brussel, Pleinlaan 2, B-1050 Brussels, Belgium

Received July 20, 1998. Revised Manuscript Received February 3, 1999

Abstract: The 9*R*,12*S*-$[tBu_2Sn]_2O$ derivative of the macrolide antibiotic erythromycin A (ErySn-A) is obtained as the sole regio- and stereospecific reaction product from the condensation reaction of $(tBu_2SnOPr)_2O$ with erythromycin A in benzene solution. Complete resonance assignments were achieved, and the covalent structure was derived using various one-dimensional and two-dimensional NMR techniques, including gradient enhanced $^1H-^{119}Sn$ heteronuclear multiple quantum correlation and heteronuclear multiple bond correlation spectroscopy. A total of 64 nuclear Overhauser effect-based distance restraints were used in restrained molecular dynamics simulations within the extensible systematic force field. This yielded a unique, well-defined conformation for ErySn-A, which was validated against 17 $^3J(^1H-^1H)$ and 21 $^3J(^{13}C-^1H)$ experimental coupling constants. Complete stereospecific assignment of the diastereotopic *tert*-butyl groups as well as the identification of the absolute configuration at C9 was achieved. The lactone ring features a tricyclic structure, with the $-O-Sn(tBu)_2-O-(tBu)_2Sn-O-$ organotin moiety covalently linked to the C9 and C12 carbons of the lactone macrocycle, and a ketal ring involving C9 with C6. The conformation of the lactone ring is strongly affected by the derivatization, but both sugar residues retain very similar conformations as compared to erythromycin A. The structure also involves a peculiar hydrogen bond between the 11-OH and the distannoxane oxygen, in which the hydrogen atom appears to be delocalized.

Introduction

In addition to cis-platinum-based drugs used in clinical cancer treatment,[1,2] and some of its derivatives with less severe side effects,[3,4] many organotin compounds likewise display significant antitumor activity in vitro[5−7] and even in vivo.[8−10] In contrast to platinum compounds, however,[2,11] no significant investigations have been reported on the relationship between the antitumor activity of organotin compounds and their intermolecular interactions with bio-organic structures. The lack of clear guidelines in the development of new tin-based antitumor compounds requires a more targeted strategy. One option is to include organotin moieties into well-studied bio-organic structures, such as steroids,[12] which might lead to facilitated delivery of the tin moiety to, and possibly help in the identification of, their interaction site. A necessary prerequisite to such a strategy is a good knowledge of structures and conformations of bio-organotin compounds, which remain rather uncommon. In the above contexts, the well-known antibiotic erythromycin A (Ery-A)[13−15] is of potential interest in organotin chemistry. A di-*n*-butyltin derivative of Ery-A, synthesized a decade ago,[16] displayed antitumor activity in vitro under conditions where Ery-A did not. However, limited stability, spectral complexity, and the lack of suitable modeling tools for conformational analysis restricted its structural characterization. We now have available a more stable and still active di-*tert*-butyltin derivative of Ery-A (hereafter called ErySn-A) to address these structural and conformational issues.

Incorporating the organotin moiety into Ery-A opened the major challenges of the covalent structure elucidation as well as the complete conformational analysis of the tin derivative, ErySn-A. An approach to address the first challenge was

* To whom correspondence should be addressed.
† High-Resolution NMR Center.
‡ General and Organic Chemistry Department.

(1) Rosenberg, B.; Van Camp, L.; Trosko, J. E.; Mansour, V. H. *Nature* **1969**, *222*, 385−386.
(2) Bloemink, J.; Reedijk, J. In *Metal Ions in Biological Systems*, Vol. 32; Sigel, A., Sigel H., Eds.; Marcel Dekker Inc: New York, NY, 1996; pp 641−685.
(3) Sherman, S. E.; Lippard, S. J. *Chem. Rev.* **1987**, *87*, 1153−1181.
(4) Berners-Price, S. J.; Sadler, P. J. *Coord. Chem. Rev.* **1996**, *151*, 1−40.
(5) Narayanan, L.; Nasr, M.; Paul K. D. *Tin Based Antitumor Drugs* **1990**, 201−217.
(6) Gielen, M. *Coord. Chem. Rev.* **1996**, *151*, 41−51.
(7) Gielen, M.; Willem, R.; Bouhdid, A.; de Vos, D.; Kuiper, C. M.; Veerman, G.; Peeters, G. J. *Oncol. Rep.* **1996**, *3*, 583−587.
(8) Gielen, M.; Willem, R.; Biesemans, M.; Bouhdid, A.; de Vos, D.; Kuiper, C. M.; Veerman, G.; Peeters, G. J. *In Vivo* **1995**, *9*, 59−64.
(9) Crowe, J.; Smith, P. J.; Atassi, G. *Inorg. Chim. Acta* **1984**, *93*, 179−184.
(10) Crowe, J.; Smith, P. J.; Cardin, C. J.; Parge, H. E.; Smith, F. E. *Cancer Lett.* **1984**, *24*, 45−48.
(11) Sundquist W. I.; Lippard, S. J. *Coord. Chem. Rev.* **1990**, *100*, 293−322.
(12) (a) Pan, H.; Willem, R.; Meunier-Piret, J.; Gielen, M. *Organometallics* **1990**, *9*, 2199−2201. (b) Gielen, M.; Lelieveld, P.; de Vos, D.; Pan, H.; Willem, R.; Biesemans, M.; Fiebig, H. H. *Inorg. Chim. Acta* **1992**, *196*, 115−117. (c) Kayser, F.; Biesemans, M.; Pan, H.; Gielen, M.; Willem, R. *Magn. Reson. Chem.* **1992**, *30*, 877−882. (d) Kayser, F.; Biesemans, M.; Gielen, M.; Willem, R. *J. Magn. Reson. Ser. A* **1993**, *102*, 249−252. (e) Kayser, F.; Biesemans, M.; Pan, H.; Gielen, M.; Willem, R. *J. Chem. Soc., Perkin Trans. 2* **1994**, 297−301.
(13) *Macrolide Antibiotics, Chemistry, Biology and Practice*; Omura, S., Ed.; Academic Press: Orlando, FL, 1984.
(14) Washington, J. A., II; Wilson, W. R. *Mayo Clin. Proc.* **1985**, *60*, 189−271.
(15) Malmborg, A.-S. *J. Antimicrob. Chemother.* **1986**, *18*, 293−296.
(16) Gielen, M.; Willem, R.; Mancilla, T.; Ramharter, J.; Joosen, E. *Si, Ge, Sn Pb Compds.* **1986**, *9*, 349−365.

10.1021/ja982559t CCC: $18.00
Published on Web 03/23/1999

initiated previously[17] through the development of two-dimensional (2D) gradient-enhanced (ge)-$^{1}H-^{119}Sn$ heteronuclear multiple quantum correlation (HMQC) and heteronuclear multiple bond correlation (HMBC) spectroscopy. This work evaluated the merits of these techniques in localizing the organotin moiety through $^{n}J(^{1}H-^{119}Sn)$ correlations.[17] The second challenge was due to the lack in the well-established force fields[18] of suitable parameters relevant to the organotin fragment. The present paper both meets the latter challenge and refines the former one, as it reveals novel covalent structural features in ErySn-A that can only be outlined from the combined strategy based on further NMR data (nuclear Overhauser effect (NOE)-based distances, $^{3}J(^{1}H-^{1}H)$ and $^{3}J(^{1}H-^{13}C)$ coupling constants) and restrained molecular dynamics (rMD) proposed here. This was made possible by the recent introduction of the new generalized extensible systematic force field (esff),[19] developed specifically to extend computational simulations to inorganic and organometallic compounds. Therefore, while situated in the broad frame of antitumor organotin compounds,[5−7] this work is mainly intended to demonstrate that molecular dynamics tools are now available to address, when combined with advanced NMR techniques, the structure and conformation of complex bio-organometallic compounds. While illustrated here, to the best of our knowledge, for the first time in a bio-organotin compound, our methodology is sufficiently general to be applicable to any organometallic compound with heavy hetero elements, being even more useful when the metal is amenable to spin $^{1}/_{2}$ NMR.

Results and Discussion

NMR Assignment and Covalent Structure Determination. Ery-A reacts at room temperature with $(tBu_2SnOPr)_2O$, obtained in situ from $(tBu_2SnO)_3$ and propanol in refluxing benzene.[21] The Ery-A molecule contains five hydroxyl functions which are potentially suitable pairwise targets for organotin condensation. The reaction features an unexpected, very high degree of regio- and stereospecificity since only a single, NMR spectroscopically pure compound, ErySn-A, is obtained. It displays two ^{119}Sn resonances at −234 and −294 ppm (Sn(a) and Sn(b), respectively),[17] each with unresolved $^{2}J(^{119}Sn-O-^{119/117}Sn)$ coupling satellites of ∼110 Hz, indicating the presence of a Sn−O−Sn moiety. As compared to that of Ery-A,[21] the ^{1}H spectrum of ErySn-A displays four additional, equally intense singlet resonances with $^{3}J(^{1}H-^{119/117}Sn)$ coupling satellites of ca. 100 Hz, assigned to the four pairwise diastereotopic tBu groups. Together these data indicate the presence of a $-(tBu)_2Sn-O-Sn(tBu)_2-$ moiety, but they do not localize its incorporation site into Ery-A. This incorporation from the condensation reaction of $(tBu_2SnOPr)_2O$ with Ery-A necessarily involves two hydroxylic functions from the latter. The question is, which ones?

The complete assignment of the ^{1}H and ^{13}C resonances of ErySn-A (Table 1) was obtained through 2D homonuclear and ge-$^{1}H-^{13}C$ HMQC[22,23] and HMBC[23,24] correlation techniques in combination with chemical shift and $^{1}J(^{1}H-^{13}C)$ scalar coupling multiplicity information obtained from 1D ^{13}C and DEPT-^{13}C spectra.[25] The ^{1}H and ^{13}C resonances of both sugar residues and the C1−C5 part of the lactone ring appear at frequencies comparable to those of Ery-A,[21] excluding the

Table 1. ^{1}H, ^{13}C, and ^{119}Sn Resonance Assignments of ErySn-A in Benzene and Comparison with Those Observed for Ery-A[21]

	ErySn-A		Ery-A	
position	δ ^{1}H ($^{n}J(^{1}H-^{119}Sn)$)	δ ^{13}C ($^{n}J(^{13}C-^{117/119}Sn)$)[b]	δ ^{1}H	δ ^{13}C
1		178.7		175.8
2	3.15	45.9	3.00	45.4
3	4.51	79.4	4.25	80.7
4	2.51	42.4	2.22	40.2
5	3.83	85.9	3.78	84.1
6		85.6		74.9
7eq (*pro-S*)[a]	2.62	45.1	2.03	39.2
7ax (*pro-R*)[a]	2.45	45.1	1.83	39.2
8	2.40	45.3	2.70	45.2
9		115.5 (52)		220.8
10	2.19	40.2	3.08	38.4
11	4.48 (27)	75.1	4.15	69.5
12		74.2 (32)		74.9
13	5.00	83.0	5.52	77.4
14a (*pro-S*)[a]	2.37	23.0	2.13	21.9
14b (*pro-R*)[a]	1.74	23.0	1.59	21.9
Me15	1.13	11.4	0.98	11.1
Me16	1.33	15.3	1.25	16.2
Me17	1.48	12.8	1.50	9.6
Me18	2.13	33.3	1.55	26.9
Me19	1.28	18.5	0.83	18.1
Me20	1.22	12.4	1.28	12.3
Me21	1.41	20.7	1.24	16.7
1′	4.53	104.5	4.65	103.8
2′	3.43	70.8	3.37	71.2
3′	2.27	66.3	2.32	66.3
4′eq(*pro-S*)[a]	1.20	29.2	1.22	29.0
4′ax(*pro-R*)[a]	0.95	29.2	0.91	29.0
5′	3.33	69.3	3.48	69.0
Me6′	1.16	21.6	1.16	21.6
Me7′Me8′	1.90	40.2	1.88	40.1
1″	5.36	96.9	4.98	96.8
2″eq(*pro-S*)[a]	2.14	35.3	2.06	35.0
2″ax(*pro-R*)[a]	1.15	35.3	1.16	35.0
3″		73.2		72.9
4″	3.01	78.5	3.00	78.3
5″	4.34	65.9	4.22	66.1
Me6″	1.62	18.7	1.59	19.3
Me7″	0.92	21.6	1.00	21.5
Me8″	3.11	49.4	3.14	49.4

	δ ^{1}H	δ ^{13}C	δ ^{119}Sn	ssa[a]
tBu1(CH_3)	1.37 (99)	30.8[c]	−234	*pro-R*
tBu2(CH_3)	1.34 (99)	31.1[c]	−234	*pro-S*
tBu3(CH_3)	1.56 (105)	30.5[c]	−294	*pro-S*
tBu4(CH_3)	1.30 (107)	31.3[c]	−294	*pro-R*
tBu1(C)		37.8[c]		
tBu2(C)		38.6 (574/607)		
tBu3(C)		39.1 (560/593)		
tBu4(C)		41.9[c]		

[a] Stereospecific assignment (ssa) of prochiral groups. [b] Single value when $^{n}J(^{13}C-^{117/119}Sn)$ satellites are unresolved. [c] Not visible because of overlap.

(17) Martins, J. C.; Kayser, F.; Gielen, M.; Willem, R.; Biesemans, M. *J. Magn. Reson.* **1997**, *124*, 218−222.

(18) (a) Némethy, G.; Pottle, M. S.; Sheraga, H. A. *J. Phys. Chem.* **1983**, *87*, 1883−1887. (b) Weiner, S. J.; Kollmann, P. A.; Case, D. A.; Singh, C.; Ghio, C.; Alagona, G.; Proteta, S.; Weiner, P. *J. Am. Chem. Soc.* **1984**, *106*, 765−784. (c) Brooks, B. R.; Bruccoleri, R. E.; Olafson, B. O.; States, D. J.; Swaminathan, S.; Karplus, M. *J. Comput. Chem.* **1983**, *4*, 187−198. (d) Dauber-Osguthorpe, P.; Roberts, V. A.; Osguthorpe, D. J.; Genest, M.; Hagler, A. T. *Proteins: Struct., Funct. Genet.* **1988**, *4*, 1243−1252.

(19) (a) Barlow S.; Rohl, A. L.; Shengua S.; Freeman, C. M.; O'Hare, D. *J. Am. Chem. Soc.* **1996**, *118*, 7578−7592. (b) Shengua, S.; Yan, L.; Yang, Y.; Shaulsky, J. *Biosym Solutions* **1995** (August), 8−11.

(20) Davies, A. G.; Kleinschmidt, D. C.; Palan, P. R.; Visishtha, S. C. *J. Chem. Soc. C* **1971**, 3972−3976.

(21) Martins, J. C.; Willem, R.; Biesemans, M. Submitted.

(22) Bax, A.; Griffey R.; Hawkins, B. L. *J. Magn. Reson.* **1983**, *55*, 301−315.

(23) Keeler, J.; Clowes, R.; Davis, A. L.; Laue, E. D. *Methods Enzymol.* **1994**, *239*, 145−207.

(24) Bax, A.; Summers, M. F. *J. Am. Chem. Soc.* **1986**, *108*, 2093−2095.

(25) On the longer term, very slow hydrolysis of the compound occurs. Minor resonances resulting herefrom match those of erythromycin A.

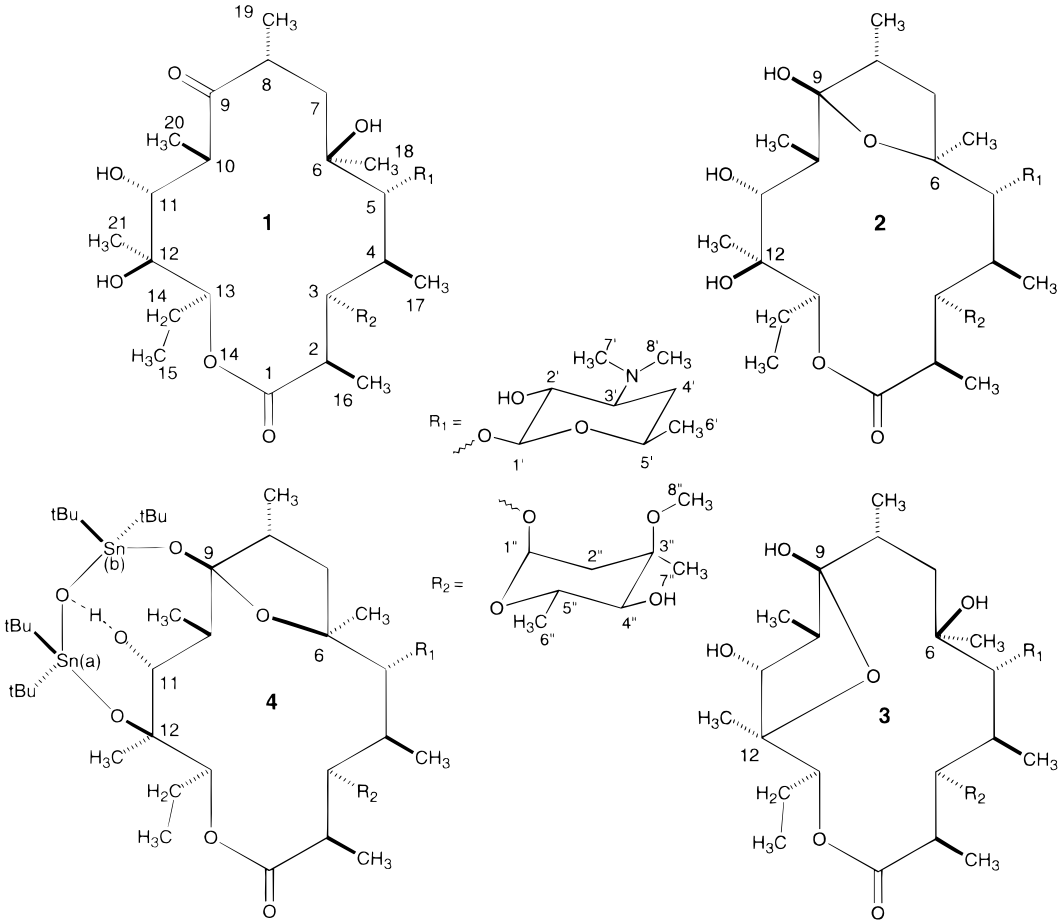

Figure 1. Chemical structures of erythromycin A (Ery-A, **1**), the [9,6] hemiketal of Ery-A (9-deoxo-6-deoxy-9*S*-hydroxy-[6,9]-epoxy-erythromycin A, **2**), the [9,12] hemiketal of Ery-A (9-deoxo-12-deoxy-9*S*-hydroxy-[9,12]-epoxy-erythromycin A, **3**), and ErySn-A, or the [9*R*,12*S*]-[$tBu_2Sn]_2O$ derivative of 9-deoxo-6-deoxy-9*S*-hydroxy-6,9-epoxy-erythromycin A (**4**). The desosamine and cladinose sugar residues are indicated as R_1 and R_2, respectively.

involvement of the 2′- and 4″-OH groups. This is independently confirmed by the observation of H/D isotope shifts in ^{13}C secondary isotope multiplet of partially labeled entities (SIMPLE)[26] spectra for both C2′ (−0.102 ppm) and C4″ (−0.127 ppm). Important modifications in the ^{13}C chemical shifts of ErySn-A with respect to those of Ery-A are confined to the C6−C13 part of the macrocycle. The quaternary C9 carbon, originally at 220.5 ppm for Ery-A, was assigned at 115.5 ppm for ErySn-A from $^2J(^1H-^{13}C)$ HMBC correlations with H8 and H10, respectively. This indicates the conversion of the C9 carbonyl into a ketal functionality. Another noticeable change includes the low-frequency shift of 10.7 ppm for C6, indicating possible involvement of the C6-OH group in either ketal ring formation or derivatization. The ^{13}C resonance of the lactone carbonyl is not affected. Thus, the condensation reaction must involve hydroxyl functionalities of the lactone macrocycle.

The key observation of the conversion of C9 from a carbonyl to a ketalic carbon can only be explained by the involvement of a hemiketalic OH group at C9 from either the [9,6] (**2**) or the [9,12] (**3**) hemiketal isomers of Ery-A **1** (Figure 1). However, only with the efficient detection of scalar long-range couplings between ^1H and ^{119}Sn nuclei, from several 2D ge-$^1H-^{119}Sn$ HMQC and HMBC spectra,[17] completed with ^{13}C and ^{119}Sn SIMPLE experiments,[26] could the final structure be proposed. The $^1H-^{119}Sn$ coupling correlation data and the $^nJ(^{13}C-^{119/117}Sn)$ coupling constants establish that the C7−C13 ^1H and ^{13}C nuclei are correlated to either one or both of the ^{119}Sn nuclei. More specifically, a large 27-Hz coupling splitting is observed between the H11 proton and the $^{119}Sn(a)$ nucleus. Other, unresolved long-range $^nJ(^1H-^{119}Sn)$ correlations connect the $^{119}Sn(a)$ resonance with the H13, Me21, and H10 resonances. The $^{119}Sn(b)$ nucleus displays correlations with the H11, H10, H8, H7ax, Me19, and Me20 protons and a very weak one with the Me21 ones. This network of long-range $^nJ(^1H-^{119}Sn)$ correlations can be accounted for by structure **4** (Figure 1), which arises from condensation of the [9,6] hemiketal isomer **2** with $(tBu_2SnOPr)_2O$. An alternative, involving the [9,12] hemiketal isomer **3** and the organotin moiety linked to the lactone ring via the C6 and C9 carbons, cannot account for the large 27-Hz coupling constant between H11 and Sn(a). This would also imply strong correlations between $^{119}Sn(a)$ and H7ax, H7eq, Me18, and H5, which are not observed.

Finally, structure **4** agrees with the equally intense $^1H-^{119}Sn$ correlations between a hydroxyl resonance at 1.17 ppm and both ^{119}Sn resonances, as well as with the observation of similar ^{119}Sn H/D isotope shifts from ^{119}Sn SIMPLE experiments[26] (Sn(a), −0.220 ppm; Sn(b), −0.251 ppm). The hydroxylic nature of this proton resonance was identified from its disappearance upon addition of a D_2O drop. The sharp resonance, SIMPLE effects, and correlations match the proposal that, in **4**, the 11-OH is placed somehow halfway between the tin atoms. Also, strong and equally intense $^1H-^{119}Sn$ coupling correlations of 11-OH are unlikely to originate from $^5J(^1H-^{119}Sn(a))$ and $^6J(^1H-^{119}Sn(b))$ couplings. The presence of a

(26) Christofides, J. C.; Davies, D. B. *J. Am. Chem. Soc.* **1983**, *105*, 5099−5105.

Table 2. Relevant Experimental $^3J(^1H-^1H)$ Coupling Constants Observed in ErySn-A in C_6D_6 and Comparison with Those of Ery-A

	ErySn-A	Ery-A[a]	rMD[b]		ErySn-A	Ery-A[a]	rMD[b]
J_{23}	4.0	9.2	1.7	$J_{1''2''eq}$	<2.0	0.9	2.4
J_{34}	4.0	1.5	1.4	$J_{4''5''}$	9.7	9.2	10.2
J_{45}	7.4	7.7	10.2	$J_{1'2'}$	7.2	7.2	10.2
J_{7ax8}	7.6	10.7	7.4	$J_{2'3'}$	10.1	10.2	10.3
J_{7eq8}	3.3	1.8	4.1	$J_{3'4'ax}$	7.5[c]	12.2	10.2
J_{1011}	<2.0	1.4	2.3	$J_{3'4'eq}$	4.0	3.6	2.9
J_{1314a}	10.4	10.9	10.3	$J_{4'ax5'}$	10.2	10.7	10.1
J_{1314b}	2.0	2.3	2.5	$J_{4'eq5'}$	2.1	1.9	3.2
$J_{1''2''ax}$	4.6	4.8	3.8				

[a] Taken from ref 21. [b] Calculated for ErySn-A from the lowest energy conformer using the Karplus equation with coefficients $A = 7.76$, $B = -1.10$, and $C = 1.40$.[31] [c] Questionable because of complex pattern.

hydrogen bridge, as shown in Figure 1, assigning the equal correlations as $^2J(^1H-^{119}Sn)$ coupling pathways, is the only reasonable explanation, being reinforced by the joined presence of H/D isotope shifts of both ^{119}Sn resonances and the rather small one of the $^{13}C11$ resonance (-0.023 ppm).

Somewhat cumbersome is the fact that, with structure **4**, the 27-Hz coupling between H11 and $^{119}Sn(a)$ is to be assigned as a $^4J(^1H-^{119}Sn)$ coupling. An alternative structure to **4**, **4′**, where the tin atom Sn(a) would be linked to the oxygen atom of C11 rather than C12, cannot be excluded at this point. In this case, H11 and $^{119}Sn(a)$, coupled through a $^3J(^1H-^{119}Sn)$ coupling, seemingly match better the observed 27-Hz coupling size. This implies the recognition of a $^7J(^1H-^{119}Sn)$ correlation, so far unknown, between Sn(a) and the protons of Me21. In our experience, supported by literature data,[27] a 27-Hz coupling size seemed unusually large for a $^4J(^1H-^{119}Sn)$, and therefore the alternative structure **4′** proposed earlier seemed reasonable.[17] Discrimination between **4** and **4′** could be achieved only after acquisition of further NMR data (NOE contacts and $^3J(^1H-^1H)$ and $^3J(^{13}C-^1H)$ coupling constants), which enabled restrained MD calculations. The analysis below shows that structure **4** emerges, so that the 27-Hz coupling splitting is, indeed, associated with a $^4J(^1H-^{119}Sn)$ coupling constant.

Conformation of ErySn-A. Analysis of the NMR data based on the assignments in Table 1 yielded 17 $^3J(^1H-^1H)$ and 21 $^3J(^1H-^{13}C)$ coupling constants (Tables 2 and 3) and a total of 64 nontrivial NOEs. The proton pairs constrained by these NOEs are distributed over all parts of the structure. They include 28 intra-lactone NOEs, of which 13 are nonvicinal, 9 NOEs occurring within the cladinose and 8 NOEs within the desosamine sugar residues, 3 intersugar NOEs, and 11 NOEs indicating close contacts between the lactone with either the cladinose (6 NOEs) or desosamine (5 NOEs) sugar residues. In addition, 5 NOEs were identified between the macrolide and the tBu groups in the organotin moiety. These data made stereospecific assignment of all CH_2 diastereotopic protons possible, allowed us to establish that both sugar residues adopt the same chair conformations as in Ery-A,[21] and served as restraints for the determination of the solution conformation of ErySn-A by rMD simulations. The presence of the organotin moiety, however, precluded the use of well-established force fields designed to model peptides,[18a] proteins,[18b,c] nucleic acids[18b,c] or organic compounds in general, such as the consistent valence force field (cvff).[18d] These lack the necessary parametrization and mathematical expressions to straightforwardly process organometallic compounds in general. More specifically, no parametrization specific for tin atoms has, to the best of our knowledge, been presented for existing force fields. We therefore turned to the recently released extensible systematic

Table 3. Comparison of Relevant Experimental $^3J(^{13}C-^1H)$ Measured in C_6D_6 for ErySn-A and Ery-A, and Calculated from the rMD-Derived Structure of ErySn-A[a]

	ErySn-A	Ery-A[b]	rMD[c]		ErySn-A	Ery-A[b]	rMD[c]
				Lactone			
J_{C4H2}	4.0	3.8	4.5	J_{C17H5}	<2.5		0.5
J_{C1H3}	4.2	3.2	4.9	J_{C18H5}	2.8		5.2
J_{C5H3}	3.1	3.5	3.6	J_{C9H7eq}	4.2		5.4
J_{C16H3}	4.8		4.8	$J_{C18H7ax}$	4.2		3.5
J_{C17H3}	6.6		6.6	J_{C9H11}	2.7	3.7	5.4
J_{C3H5}	4.4	5.5	2.8	J_{C13H11}	4.1	2.8	2.6
J_{C7H5}	<2.5		1.7				
				Glycosidic			
$J_{C3H1''}$	4.1	4.6	3.7	$J_{C5H1'}$	2.5	3.9	3.0
$J_{C1''H3}$	5.8	4.6	3.2	$J_{C1'H5}$	6.0	6.5	4.5
				Cladinose			
$J_{C3''H1''}$	5.5	5.7	6.7	$J_{C5''H1''}$	6.2	6.7	6.8
				Desosamine			
$J_{C3'H1'}$	<2.5	<2.5	1.3	$J_{C5'H1'}$	<2.5	<2.5	1.5

[a] Large and small coupling constant values are well reproduced in the conformation obtained from rMD. Exceptions are found in the Karplus function dihedral angle intervals where $dJ/d\theta$ is large or where the application of this equation can be questioned because the nature of the atoms involved differs significantly from those used in the glycosidic parametrization set.[33] [b] Taken from ref 21. [c] Calculated from the lowest energy conformer using the Karplus equation with coefficients $A = 5.7$, $B = -0.6$, and $C = 0.5$[33]

force field (esff),[19] which is specifically designed to meet the growing need to model inorganic and organometallic compounds. Its mathematical formulation, and the use of a modest set of atomic parameters from which the complete molecular force field is generated through a series of empirical rules, provide the basis needed to adequately deal with the broad compositional and geometrical diversity of organometallic compounds.[19] Prior to its use for the structure determination of ErySn-A, the esff was assessed by performing a comparative structure determination of Ery-A with restrained MD using both the esff[19] and the well-established cvff.[18d] The otherwise identical protocols[21] produced essentially identical conformations, demonstrating that the treatment of organic molecular structures by the esff provides equally reliable results as that with the standard force fields.

Practically speaking, restrained MD simulations of ErySn-A were further complicated by the new chiral spiranic center at C9 generated upon synthesis of ErySn-A and by the lack of stereospecific assignments for the diastereotopic tBu groups (Figure 1). The NMR data indicate the presence of a single stereoisomer. The parallel rMD simulations performed for the possible 9*R* and 9*S* stereoisomers of ErySn-A, using all NOE-based distance restraints except those involving the tBu groups,[28,29] unambiguously favor the 9*R* configuration[30] and dismiss the 9*S* one. Conformers generated from the rMD simulations for the 9*R* isomer satisfied all restraints to within 0.2 Å. This contrasts with the 9*S* isomer, where 33 lower energy conformations among a total of 50 consistently displayed nine restraint violations in excess of 0.2 Å, and even three over 0.5 Å, with an averaged maximum violation of 0.61 Å. Violations occurred all over the structure but were most pronounced for interproton

(27) Wrackmeyer, B. *Annu. Rep. NMR Spectrosc.* **1995**, *16*, 73−186.

(28) Although these could have been imposed by means of pseudoatoms,[29a] their definition at the geometrical center of the diastereotopic tBu groups was expected to severely decrease the information content of the restraints.[29b]

(29) (a) Wüthrich, K.; Billeter, M.; Braun, W. *J. Mol. Biol.* **1983**, *169*, 949−961. (b) Güntert, P.; Braun, W.; Billeter, M.; Wüthrich, K. *J. Am. Chem. Soc.* **1989**, *111*, 3997−4004.

(30) Simply substituting the hydrogen of the OH group of the hemiketal in the 9*S* isomer **2** for a tin atom, keeping identical relative configurations for the C9 carbon, modifies the absolute configuration of the C9 atom from *S* to *R*.

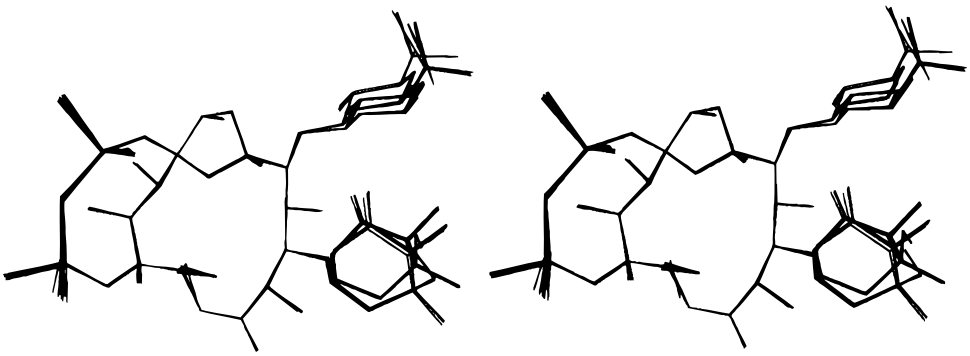

Figure 2. Structure of ErySn-A in stereoview, as represented by the group of 21 low-energy rMD conformers which satisfy the experimental distance constraints. All non-hydrogen atoms, except the internal rotation-related methyl carbons of the four tBu groups, were considered for superposition. These were also omitted from the figure for clarity. Conformers 2−21 are each superimposed on conformer 1 such that minimal rmsd is achieved for the atoms that constitute the lactone macrocycle (C1 to O14).

contacts within the lactone ring. More evidence favoring 9*R* over 9*S* came from the distance restraints involving the tBu groups. For each pair of diastereotopic tBu groups, both stereospecific assignments were considered, and each NOE-derived distance restraint involving the tBu groups was matched with the corresponding distances in the conformations obtained from rMD. For the 9*S* isomer, all distances were severely violated, irrespective of the stereospecific assignment, and violations ranged in size up to 5.9 Å. This could not be improved through rMD simulations for any of the possible assignments. By contrast, in the 9*R* stereoisomer, two out of six restraints were immediately satisfied for one stereospecific assignment, and subsequent rMD simulations including these distance restraints produced structures which satisfied all distance restraints to within 0.5 Å. Additional support for the 9*R* stereoisomer is also provided by the average internal energy of 50 free MD conformers of ErySn-A with 9*R* configuration (108.0 ± 5.1 kcal mol^{-1}), which is significantly lower than that observed for those with 9*S* configuration (146.5 ± 6.0 kcal mol^{-1}). Inversion of the absolute configuration at C9 is accompanied by more repulsive contacts, as evidenced by the considerably higher van der Waals energy for the 9*S* stereoisomer (50.7 ± 3.3 kcal mol^{-1}) as compared to that for the 9*R* one (37.0 ± 2.9 kcal mol^{-1}). Finally, the low-energy rMD conformers of the 9*R* isomer consistently reproduce the 11-OH bridge with the distannoxane oxygen, while those of the 9*S* isomer do not.

From the 50 starting conformers of the 9*R* isomer, 45 structures yielded low-energy conformers, ranging from 173.1 to 179.2 kcal mol^{-1}. Of these, 21 conformers satisfied all distances to within 0.5 Å, with on average only two violations in the 0.2−0.5 range; hence, they represent the structure of ErySn-A in benzene solution (Figure 2). The statistics of restraint violation and the breakdown of the energies of all 21 accepted conformers are collected in Table 4.

These structures were further validated against the $^3J(^1H-^1H)$ and $^3J(^{13}C-^1H)$ coupling constant data, which were not imposed during the rMD simulations. $^3J(^1H-^1H)$ coupling constants calculated[31] from the lowest energy conformer of ErySn-A compare generally well with the experimental ones (Table 2). Comparison of the $^3J(^{13}C-^1H)$ coupling constants measured from the 2D ge-J-HMBC[32] experiment with those calculated[33] from the structure (Table 3) is more difficult, as only an approximate Karplus equation is available. Given its qualitative nature, the agreement between the experimental and calculated $^3J(^{13}C-^1H)$ coupling constants is, in general, fair.

Table 4. Statistics of Distance Restraint Violations and Energy Breakdown for the 21 Low-Energy Conformers Obtained for ErySn-A by rMD within the Extensible Systematic Force Field

Restraint Violations			
no. >0.1 Å[a]	7.9 ± 0.9		
sum[b] (Å)	2.4 ± 0.1		
max[c] (Å)	0.4 ± 0.1		
Energy Breakdown (kcal mol^{-1})			
total energy	175.2 ± 1.3	Coulomb energy	-19.5 ± 0.9
internal energy	112.2 ± 1.8	restraint energy	20.3 ± 0.8
non bond energy	43.1 ± 1.1	distance restraint	15.7 ± 1.0
vdW energy	62.2 ± 0.6	chiral restraints	4.6 ± 0.3

[a] Average number of violations larger than 0.1 Å. [b] Average sum of all violations. [c] Average maximum violations occurring within the low-energy conformers.

The conformation of ErySn-A is very well defined (Figure 2). The complete macrolide ring, including the exocyclic organotin ring, displays a unique conformation, the average pairwise root-mean-square deviation (rmsd) being only 0.053 ± 0.001 Å. By contrast, the sugar residues show conformational heterogeneity into two subsets within the group of low-energy structures. This suggests that, within the boundaries of the energy surface minimum defined by the esff and the restraints, two equi-energetic local minima satisfy all data (see Figure 2). As a result, the average rmsd for all the atoms, excluding hydrogens and tBu methyl carbons, is somewhat higher, at 0.25 ± 0.07 Å.

The 14-atom macrolide, the endocyclic [9,6] ketal, and the exocyclic [9,12] organotin rings being all joined via the spiranic C9 atom of ErySn-A, the derivatization strongly determines the overall conformation of the original macrocycle (Figure 3 and Table 5). Most dihedral angles within the lactone ring have rotated by at least 60°, seven even over 120°, when compared to the solution conformation of Ery-A,[21] making the lactone ring in ErySn-A more concave than that in Ery-A. In Ery-A,[21] close proximity is observed only for the H4−H10 and H4−H11 intralactone distances of 2.85 and 2.32 Å, respectively. In ErySn-A, the H4−H10 distance is shortened to 2.36 Å, while the H4−H11 distance has increased to as large as 4.44 Å. The distant interproton pairs H2−H10 and H3−H10 in Ery-A reduce from 4.07 to 2.79 and from 5.19 to 3.98 Å, respectively. The mean plane of the exocyclic organotin moiety and the C1−C6 part of the lactone ring are more or less coplanar. The endocyclic ketal five ring adopts an envelope conformation, with the C7 atom acting as the flap and the C8−C9−O−C6 dihedral angle at 6.8°. All these conformational constraints from the tin

(31) Haasnoot, C. A. G.; De Leeuw, F. A. A. M.; Altona, C. *Tetrahedron* **1980**, *36*, 2783−2792.
(32) Willker, R.; Leibfritz, D. *Magn. Reson. Chem.* **1995**, *32*, 665−669.
(33) Tvaroska, I.; Hricovini, M.; Petrakova, E. *Carbohydr. Res.* **1989**, *189*, 359−362.

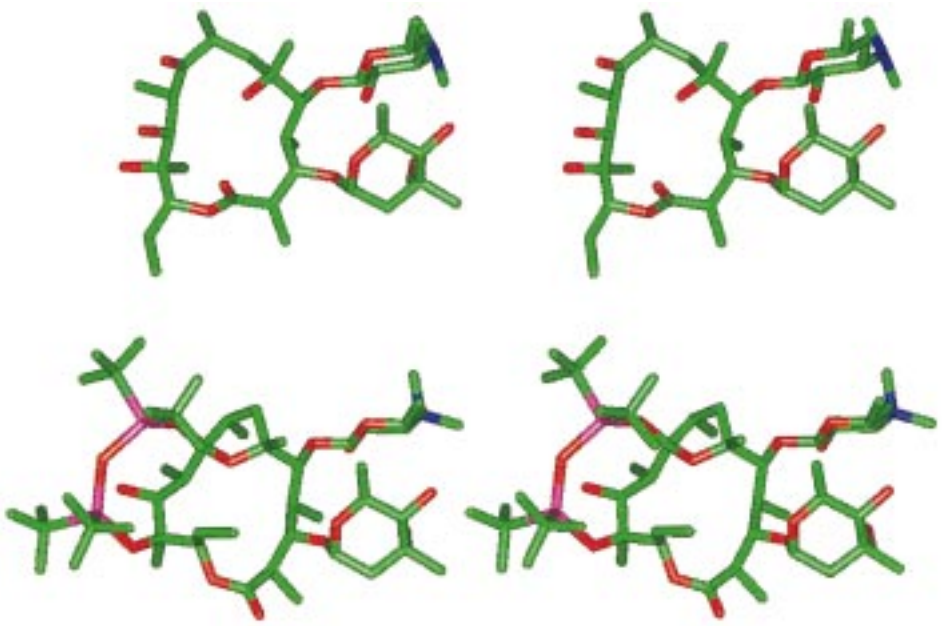

Figure 3. Stereoview representation of the lowest energy conformer of Ery-A (top) and ErySn-A (bottom) using stick models. The tin atoms are colored in purple. The conformer of Ery-A was superimposed on that of ErySn-A for minimal rmsd in the positions of the atoms that constitute the lactone macrocycle (C1 to O14) to allow for the same view of the structure. Note the large changes in side-chain orientation introduced by the organotin derivatization, as can be seen for the ethyl side chain and the adjacent lactone carbonyl, while the orientation of the sugar residues is more or less conserved.

Table 5. Dihedral Angle Comparison between the Solution Structures of ErySn-A and Ery-A in Benzene Solution

		angle (deg)	
no.	dihedral angle	ErySn-A	Ery-A[a]
1	O14−C1−C2−C3	92.7	120.4
2	C1−C2−C3−C4	−144.2	−82.1
3	C2−C3−C4−C5	155.3	159.1
4	C3−C4−C5−C6	−72.3	−91.2
5	C4−C5−C6−C7	−130.8	−75.5
6	C5−C6−C7−C8	93.2	174.9
7	C6−C7−C8−C9	43.1	−72.1
8	C7−C8−C9−C10	−150.0	−68.5
9	C8−C9−C10−C11	−164.2	119.9
10	C9−C10−C11−C12	−106.4	−166.0
11	C10−C11−C12−C13	54.4	167.2
12	C11−C12−C13−C14	−158.4	−73.2
13	C12−C13−O14−C1	137.0	110.1
14	C13−O14−C1−C2	−36.8	176.4
15	H3−C3−O3−C1″	32.0	23.2
16	C3−O3−C1″−H1″	36.4	38.3
17	H5−C5−O5−C1′	26.7	12.9
18	C5−O5−C1′−H1′	44.3	40.6

[a] Taken from ref 21.

derivatization basically turn the lactone ring inside out (Figure 3) and remove its characteristic Perun-type diamond lattice conformation.[34] The cladinose and desosamine sugars, however, retain similar orientations with respect to the lactone ring, as well as to each other (Figure 3). This is supported by the similarity in the dihedral angles of the C3−C5 part of the lactone ring and in the glycosidic angles (Table 5).

Considering the five hydroxyl functions of Ery-A, and its existence as the C9-keto form and both [9,6] and [9,12] hemiketal isomers, the regio- and stereospecificity of the tin derivatization is quite remarkable. This can be rationalized on the basis of changes in the lactone ring conformation which result from the ketalization of C9 and predispose the 12-OH and 9-OH into a configuration suitable for the reaction. The [9,6] hemiketal provides an acceptable explanation for the stereospecificity of the reaction: the X-ray structure of Ery-A already shows 6-OH and C9 to be correctly positioned for the [9,6] hemiketal formation, with the 9*S* stereochemistry[30] in Ery-A needed for the generation of the 9*R* isomer of ErySn-A.

Scheme 1

Another remarkable feature is the hydrogen bridging between the 11-OH and the distannoxane oxygen (Figure 1). The equal intensities of the strong correlations between the 11-OH proton and both ^{119}Sn nuclei, as well as the abnormally low ^{13}C SIMPLE effect at C11 contrasting the very high ^{119}Sn one at both tin atoms, support the view that this proton is essentially transferred from the 11-OH group to the distannoxane oxygen (Scheme 1). This can be viewed both as a hydrogen involved in a three-center bond and as a kind of zwitterionic structure. The latter, in turn, suggests that the distannoxane oxygen atom is very basic and can be viewed formally as an O^{2-} entity able to extrude a proton from an alcohol function.

The introduction of the endocyclic five ring and the exocyclic nine ring into the macrolide affects its dynamic behavior, as evidenced by the free MD simulations of ErySn-A. Under identical simulation protocols,[21] the order parameters describing the variance of the dihedral angles are generally higher for ErySn-A than those for Ery-A. The lactone region is also considerably less flexible than that in Ery-A. Not surprisingly, the changes are most pronounced in the C6−C10 region, at the bridgehead of the ketal ring and Sn(b), and around C12, at the bridgehead of Sn(a). The ^{13}C relaxation times of the methyl protons also indicate the conformational changes upon organotin derivatization (Table 6). Decreased relaxation times for Me18 (C6), Me21 (C12), and, to a lesser extent, Me17 (C4) indicate

(34) (a) Egan, R. S.; Perun, T. J.; Martin, J. R.; Mitscher, L. A. *Tetrahedron* **1973**, *29*, 2525−2538. (b) Egan, R. S.; Perun, T. J.; Martin, J. R.; Mitscher, L. A. *J. Am. Chem. Soc.* **1975**, *97*, 4578−4583.

Table 6. ^{13}C T_1 Relaxation Times (s) for Methyl Carbons in ErySn-A and Ery-A

methyl carbon[a]	ErySn-A	Ery-A	methyl carbon[a]	ErySn-A	Ery-A
Me15 (C14)	2.8	2.9	Me21 (C12)	0.9	1.4
Me16 (C2)	1.2	0.8	Me6′	2.6	2.1
Me17 (C4)	1.4	1.7	Me6″	2.1	1.9
Me18 (C6)	0.8	1.8	Me7″	2.3	2.1
Me19 (C8)	1.5	1.6	Me8″	3.4	4.2
Me20 (C10)	4.4	2.2			

[a] The macrocycle carbon linked to each methyl group is shown in parentheses.

reduced methyl rotor freedom in ErySn-A as compared to that in Ery-A. The opposite holds for Me16 (C2), and even more dramatically for Me20 (C10).

Unlike Ery-A, ErySn-A displays antitumor activity in vitro against cell lines of a screening panel currently used by the National Cancer Institute.[5,6,35−37] The activity, which compares moderately favorably with those of clinical reference compounds under identical screening conditions,[35] originates either from ErySn-A or from some hydrolysis product of the $[(tBu)_2Sn]_2O$ moiety, but not from Ery-A, proven to be inactive. Details are provided in the Experimental Section.

Conclusion

The first NMR and restrained MD-based three-dimensional structure determination of a bio-organotin compound in solution has been presented. This successful achievement critically depended on the combined availability of the newly developed $^1H-^{119}Sn$ HMQC and HMBC correlation techniques[17,38] and of a general force field,[19] which can incorporate organometallic moieties into the force field expression. We anticipate that such a combined NMR and restrained MD approach will be of general use in the extensive conformational study of organotin compounds. Given that many other metals, such as ^{103}Rh, ^{109}Ag, ^{113}Cd, ^{195}Pt, ^{199}Hg, and ^{207}Pb, have also favorable spin $^1/_2$ properties, NMR-based restrained MD calculations on organometallic substances with these elements should likewise be applicable.

It should be recognized that the precise relevance of such advanced conformational studies to the assessment of antitumor properties of organometallic compounds still needs to be explored. We are nevertheless convinced that mechanistic interpretations of pharmaceutical properties of antitumor drugs have an in-depth insight into their structural and conformational features as an absolute prerequisite.

While this principle is widely recognized and applied in the field of medicinal chemistry of purely organic compounds, for instance peptides,[39] such was hardly the case in organometallic compounds in general, and in bio-organotin compounds in particular. Indeed, the presence of metal atoms in these complex structures seriously hampered the development of combined NMR and rMD approaches in organometallic chemistry. We expect that the strategy outlined here will complement the considerable efforts already accomplished in platinum chemistry, with regard to the mechanism of interaction of small platinum complexes with DNA.[2−4]

Experimental Section

Synthesis, Characterization, and Biological Activity. A suspension of 300 mg (1.20 mmol) of di-*tert*-butyltin oxide in a mixture of 10 mL of *n*-propanol and 25 mL of benzene is refluxed for 2−3 h in a Dean−Stark apparatus with distillation of the ternary and subsequent binary azeotropes to ca. 50% of the initial volume.[20] The remaining solution is allowed to cool to room temperature, after which 443 mg (0.60 mmol) of Ery-A in 10 mL of benzene is added. After the solution is stirred overnight at room temperature, the solvent is slowly evaporated, leaving a white solid that proved to be NMR-pure, up to small resonances resulting, on the longer term, from traces of the free Ery-A.[25] No crystals suitable for X-ray diffraction analysis could be obtained.

Elemental Analysis. Calcd for $C_{53}H_{101}O_{14}NSn_2$ (MM 1213.85): H, 8.39; C, 52.45; N, 1.15. Found: H, 8.27; C, 52.73; N, 1.06. Electron spray mass spectrometry (cationic mode, Micromass Quattro II instrument coupled with a Masslynx system): $[C_{53}H_{101}O_{14}NSn_2]^+$; base and molecular peak,1214; $[C_{16}H_{37}O_3Sn_2]^+$, 515. IR spectroscopy (Perkin-Elmer FT-IR 1720X, KBr, cm^{-1}): 3473, bridged OH; 3670, free OH; 1731, ester C═O; 1166, OC−O; 579 (w), Sn−O−Sn.

The antitumor activity of ErySn-A was assayed in vitro, using the sulforhodamine B (SRB) protein to measure ID_{50} values in a cell viability test.[36] The human cell lines used (and ID_{50} values found, in nanograms per milliliter, for ErySn-A) were MCF7 (112), EVSAT (109), WIDR (382), IGROV (98), M19 MEL (126), A498 (137), and H226 (133). For Ery-A, ID_{50} values were all larger than 60 000, except for WIDR, where a value of 37 978 ng/mL was found, indicating a total absence of activity. The cell lines belong to the currently used anti-cancer screening panel of the U.S. National Cancer Institute.[37]

NMR Experiments. Samples were prepared by dissolving ca. 20 mg of ErySn-A (**4**) in 0.5 mL of C_6D_6 (Aldrich). All NMR experiments were performed at 303 K on a Bruker AMX500 instrument, equipped with an X32 computer, a BSMS digital lock, and a BGU II gradient unit allowing the application of B_0 gradients of up to 0.5 T m^{-1}. Operating frequencies for ^1H, ^{13}C, and ^{119}Sn were 500.13, 125.75, and 186.50 MHz, respectively. Chemical shifts were referenced to the residual solvent peak and converted to the TMS scale by adding 7.15 and 128.0 ppm for ^1H and ^{13}C, respectively. For ^{119}Sn, external referencing was used with $\Xi = 37.290\,665$ MHz.[40] 1D spectra, including ^1H,^1H-decoupled ^{13}C and distortionless enhancement through polarization transfer (DEPT)-90 and DEPT-135 ^{13}C spectra, and T_1 relaxation times acquired with the standard inversion recovery scheme, were obtained from standard pulse programs from the Bruker library. Homonuclear 2D double-quantum-filtered correlation spectroscopy (DQF-COSY),[41] total correlation spectroscopy (TOCSY),[42] and nuclear Overhauser effect spectroscopy (NOESY)[43] spectra and heteronuclear 2D ge-$^1H-^{13}C$ HMQC,[22,23] ge-$^1H-^{13}C$ HMBC,[23,24] and three-dimensional (3D) ge-$^1H-^{13}C$-J-HMBC[32] spectra were recorded as described for Ery-A.[21] The 1D and 2D $^1H-^{119}Sn$ HMQC and HMBC experiments were performed as previously described.[17,38]

Structural Data Collection. Interproton distances were determined from the build-up of the corresponding NOE cross-peak intensities measured from a series of eight NOESY spectra with mixing times of 300, 400, 500, 600, 700, 800, 1000, and 1200 ms, and recorded as described before.[21] Integration areas were defined at 500 ms with the UXNMR software and subsequently applied to all NOESY spectra. To extend the linearity of the NOE build-up, the cross-peak intensities can be normalized against the diagonal peak.[44] As considerable overlap is present, however, only a limited number of diagonal peaks are well

(35) de Vos, D.; Willem, R.; Gielen, M.; van Wingerden, K. E.; Nooten, K. *Metal Based Drugs* **1998**, *5*, 179−188.
(36) Kepers, Y. P.; Peters, G. J.; Van-Ark-Otte, J.; Winograd, B.; Pinedo, H. M. *Eur. J. Cancer* **1991**, *27*, 897−900.
(37) Boyd, M. R. *Princ. Pract. Oncol.* **1989**, *3*, 1−12.
(38) Willem, R.; Bouhdid, A.; Kayser, F.; Delmotte, A.; Gielen, M.; Martins, J. C.; Biesemans, M.; Mahieu, B.; Tiekink, E. R. T. *Organometallics* **1996**, *15*, 1920−1929.
(39) (a) Scheek, R.; van Gunsteren, W.; Kaptein, R. *Methods Enzymol.* **1989**, *177*, 204−218. (b) Kessler, H.; Seip, S. In *Two-dimensional NMR spectroscopy. Applications for Chemists and Biochemists*, 2nd ed.; Croasmun, W. R., Carlson, R. M. K., Eds.; VCH Publishers: New York, NY, 1994; pp 619−654.
(40) Davies, A. G.; Harrison, P. G.; Kennedy, J. D.; Puddephatt, R. J.; Mitchell, T. N.; McFarlane, W. *J. Am. Chem. Soc.* **1969**, *91*, 1136−1141.
(41) Piantini, U.; Sørensen, O. W.; Ernst, R. R. *J. Am. Chem. Soc.* **1982**, *104*, 6800−6801.
(42) Bax. A.; Davis, D. G. *J. Magn. Reson.* **1985**, *65*, 355−360.
(43) Jeener, J.; Meier, B. H.; Bachmann, P.; Ernst, R. R. *J. Chem. Phys.* **1979**, *71*, 4546−4553.

resolved. Therefore, individual resonances were grouped according to their T_1 relaxation time constants and normalized against a resolved diagonal peak within each group. Linear regression of the build-up curves yielded correlation coefficients well above 0.94, with most superior to 0.99, indicating linearity of the build-up. Finally, the interproton distances corresponding to each NOE were obtained through calibration of the associated slope against the slope of the CH_2 geminal NOE of carbon C7, corresponding to a distance of 1.78 Å. These distances were translated into upper limit distance restraints through multiplication by 1.1. Lower limits were set to twice the hydrogen van der Waals radius. Distance restraints involving methyl and *tert*-butyl groups were referred to the corresponding pseudoatom and increased by 0.5 and 2.4 Å, respectively. Stereospecific assignments for each of the four CH_2 moieties were obtained from the combined analysis of $^3J(^1H-^1H)$ and vicinal NOEs within the associated $-CH_2-CH-$ fragments (Table 1). $^3J(^1H-^1H)$ coupling constants were obtained from 1D ^1H spectra, processed with mild Gaussian apodization. $^3J(^{13}C-^1H)$ couplings were extracted from the 3D ge-$^1H-^{13}C$-J-HMBC spectrum as described for Ery-A.[21]

Molecular Modeling. All molecular modeling was performed using the Biosym 95.0 software package (9685 Scranton Rd., San Diego, CA), on a Silicon Graphics Indigo2 computer. Discover 3.0 was used throughout.[45] The recently developed esff was used.[19] The results were analyzed using the Analysis and Decipher modules within Biosym 95.0. All simulations were performed in vacuo. No cutoffs were considered to calculate nonbonding interactions. A dielectric constant of 2.3 (benzene) was chosen and considered distance dependent in order to (crudely) mimic solvent screening effects. Distance and torsional angle restraints were imposed using a harmonic potential function with forcing constants of 40 kcal mol^{-1} $Å^{-2}$. A suitable starting structure was generated for both the 9*R* and 9*S* stereoisomers of ErySn-A, using the previously determined NMR solution structure of Ery-A in benzene.[21] Following initial energy optimization, the starting structures of both isomers were submitted to 5 ps of free MD using random starting velocities corresponding to a Maxwell−Boltzmann distribution at 1000 K. Subsequently, a 25-ps free MD trajectory was sampled every 5 ps, yielding, for each stereoisomer, a set of 50 conformers judged to be representative of the conformational space available to ErySn-A. This group of 50 conformers was then used as starting conformations for 5-ps rMD at 1000 K, during which the distance restraints were gradually imposed through linear scaling of the associated force constants (from 0 to 1 in four steps) to full effect. Following another 5 ps of 1000 K rMD, each restrained conformer was annealed from 1000 to 300 K by lowering the temperature in steps of 100 K, followed by 1-ps rMD. At 300 K, another 5 ps of rMD was applied prior to energy optimization using a cascade of steepest descent, conjugate gradient, and Newton−Raphson energy minimization[46] until the maximum derivative dropped below 1 cal. mol^{-1} $Å^{-1}$. Chiralities were restrained at all times to avoid chirality inversion, with a force constant of 100 kcal mol^{-1} rad^{-2}.

Acknowledgment. J.C.M. is a postdoctoral research associate of the Fund for Scientific Research Flanders (Belgium). The authors are indebted to the Fund for Scientific Research Flanders (Belgium) for financial support: FKFO, Grant No. 2.0094.94; Nationale Loterij, Grant No. 9.0006.93; and FWO Grant No. G.0192.98. Prof. Dr. K. Jurkschat, Department of Inorganic Chemistry, University of Dortmund, is kindly acknowledged for providing a sample of di-*tert*-butyltin oxide.

JA982559T

(44) (a) Macura, S.; Farmer, B. T., II; Brown, L. R. *J. Magn. Reson.* **1986**, *70*, 493−499. (b) Willem, R.; Biesemans, M.; Hallenga, K.; Lippens, G.; Malaisse-Lagae, F.; Malaisse, W. J. *J. Biol. Chem.* **1992**, *267*, 210−217.

(45) *Discover 3.0.0 User Guide, Part 1*; Molecular Simulations Inc., 9685 Scranton Rd., San Diego, CA.

(46) Leach, A. R. *Molecular Modelling, Principles and Applications*; Addison-Wesley Longman: Singapore, 1996; pp 221−229.